INSTRUMENTATION

Correction for Field Nonuniformity in Scintillation Cameras Through Removal of Spatial Distortion

G. Muehllehner,* J. G. Colsher,* and E. W. Stoub

Searle Radiographics, Des Plaines, Illinois

A method to correct for the spatial distortions of gamma cameras has been developed. The method consists of two parts: measuring spatial distortions and repositioning events during accumulation. Distortions are measured using a pattern consisting of parallel slits on 15-mm centers with slit-pattern images obtained in two orthogonal orientations. Slit locations are used to determine X and Y displacements. In repositioning camera events, X and Y event coordinates are digitized and correction displacements added. The procedure is implemented in hardware that repositions each event in real time without introducing additional dead time.

Distortion removal offers considerable advantage over other uniformity-improvement schemes, since it correctly compensates for the major cause of nonuniformity, spatial distortion. The method may be used for quantitative studies, because it does not change the number of detected events.

J Nucl Med 21: 771–776, 1980

The quality of the representation of some object by an imaging device depends upon the magnitude of errors introduced by the device. The Anger scintillation camera possesses several components of such errors, mainly limited spatial resolution, spatial distortion, and variations in point-source sensitivity. Whereas the first is the result of random processes related to random fluctuations in photon distribution, the latter two are the result of systematic processes related to the camera's optical and electronic design. These systematic errors may be alleviated by either design changes or by additional data processing. In this paper we address the elimination of one of these problems, spatial distortion, by on-line data processing.

Errors caused by variations in point-source sensitivity and spatial distortion are apparent as nonuniformities in the field flood of a scintillation camera (*1*).

Variations in point source sensitivity (count rate) as a function of position on the camera face are caused by shifts in the average photopeak pulse height relative to the energy-acceptance window. These variations can result from an improper gain setting of a photomultiplier as a result of incorrect tuning, or from electronic component changes with time. They can also result from an optical design where efficiency of light collection varies as a function of position. This results in a difference in photopeak pulse height between the photomultiplier tubes. In a well-designed and properly tuned camera, such variations in point-source sensitivity can be kept to a clinically insignificant level of 1–2% (*2*).

In the case of spatial distortions, nonuniformities result from local count compression or expansion (*3*). To be visually noticeable in an image of a line-pattern phantom or a Smith orthogonal-hole pattern, such distortions must exceed several millimeters in spatial displacement; to be significant in clinical images, the distortions must be even more severe. However, distortions may cause unacceptable field-flood variations when the displacement is less than a millimeter. As an example,

* Present address: Dept. of Radiology, Hospital of the Univ. of Pennsylvania, 3400 Spruce St., Philadelphia, PA 19104.

Received Feb. 4, 1980; revision accepted April 2, 1980.

For reprints contact: G. Muehllehner, PhD, Dept. of Radiology, Hospital of the Univ. of Pennsylvania, 3400 Spruce St., Philadelphia, PA 19104.

if a circular area 20 mm in diameter is compressed by 0.4 mm toward its center from all directions (as might be the case over the center of a photomultiplier), the effective area is reduced from 100 π mm^2 to 92 π mm^2. This causes an 8% increase in count density, with a corresponding reduction in count density in the surrounding area. Thus spatial distortions cause noticeable field-flood nonuniformities well before displacements are visually apparent in line-pattern images, and indeed are the primary source of field-flood nonuniformities.

Common methods to correct for field nonuniformities in scintillation cameras increase or decrease the total counts acquired in a particular area using information from previously acquired field floods (*4,5*). Such methods do not correctly compensate for the primary causes of nonuniformities and can lead to artifacts and various related problems as described by others (*1,2,6,7*). Nonuniformities due to variations in point-source sensitivity should be corrected using the "sliding energy window" technique (*1,8*), in which the energy window is adjusted on an event-by-event basis to correct for local variations in photopeak pulse height. Nonuniformities due to spatial distortions should be corrected by removing the distortion and recording the detected event in its appropriate spatial location (*9–12,*†).

In the following sections the principle of distortion removal will be discussed in more detail, a particular implementation described,‡ and its performance evaluated as a function of various parameters.

DISTORTION REMOVAL—PRINCIPLE

Spatial distortions are systematic errors in the positioning of scintillation events. Such distortions are caused by nonlinear changes in the light distribution in the scintillator as a function of location. Since the linear Anger camera arithmetic scheme is not adequate to compensate for these effects, events are not recorded in their true location. The resulting errors (less than 1.0 mm) are small compared with the event-to-event error resulting from statistical uncertainties in the number of photons received by each photomultiplier. However, these small distortions cause visible artifacts because the displacements are applied to *all* events in a particular region.

Since distortions are systematic and change slowly with position, the errors can be corrected either through event-by-event processing during accumulation or by subsequent processing of the image.† For either technique the displacements must be known accurately. This can be achieved in three ways: by using a regular array of point sources,† by using a line pattern as a substitute for a point source (*10–12*), or by scanning a point source across the field (*13*). Since the true location is known and the actual (distorted) location in the image is measured, a correction displacement can be calculated. This calculation is performed for all source locations in the field. If these correction displacements are stored in a memory, then for each event the X and Y coordinates can be digitized, and the correction displacements can be added to the original coordinates to obtain the correct coordinates for the event.

To avoid introducing artifacts that are as severe as the errors to be corrected, processing must be done quite accurately. As stated above, displacements of 0.4 mm can produce nonuniformities up to 8%; the accuracy in the coordinate shift must therefore be a small fraction of this distance. For example, consider a large-field-of-view camera with an active diameter of 400 mm and a spatial resolution of 4 mm. To digitize an image from such a camera without significant loss of resolution requires a digitization accuracy of 1/256 of full scale, or 8 bits in binary notation. The correction accuracy should be 10% of 0.4 mm (namely, 0.04 mm, or 1/10,000 of full scale) to avoid artifacts and reduce nonuniformities to below 1%, thus resulting in a desired accuracy of approximately 13 bits in binary notation. Thus the displacement corrections need to be much more accurate than the original X and Y image coordinates because *systematic* errors that are only a small fraction of the resolution distance produce visible nonuniformities in the field flood.

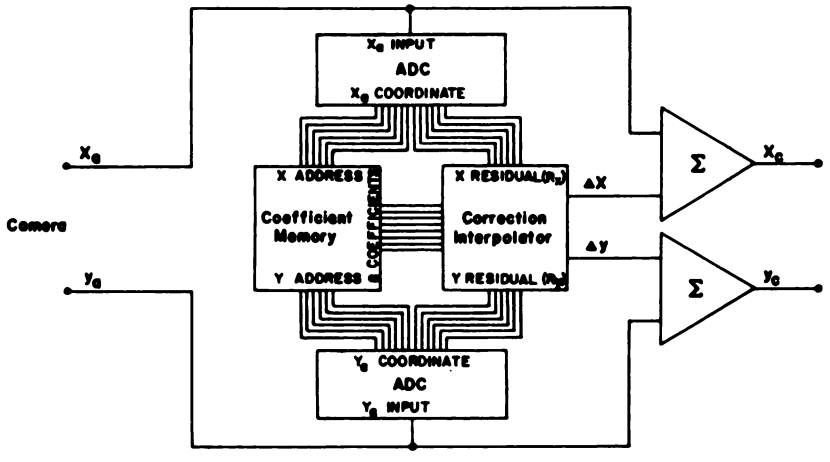

FIG. 1. Block diagram of on-line distortion-removal processor. X_a, Y_a are the coordinates as determined by the analog electronics, and X_c, Y_c are the corrected coordinates.

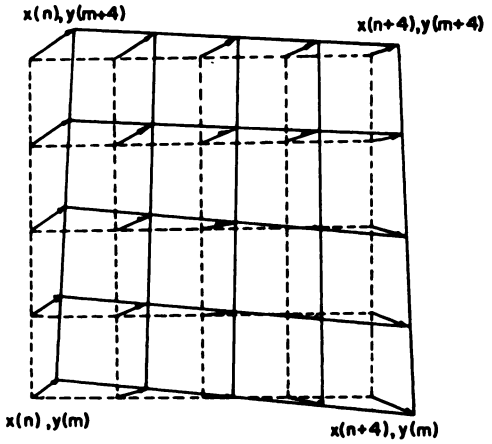

FIG. 2. Example of interpolation showing four stored corner coefficient values and interpolated values in 1/256 element size. Note change in size and shape of elements.

DISTORTION REMOVAL—IMPLEMENTATION

Event processing. Events are repositioned in real time using a hardwired processor. Figure 1 shows a block diagram of the electronics for distortion removal. The X and Y coordinates are digitized in 12-bit analog-to-digital converters (ADC); the most significant 6 bits are used as addresses to look up the correction coefficients in a 64×64 matrix. Distortions in a scintillation camera change only slowly with a frequency that is typically directly related to the photomultiplier spacing. Thus it can be assumed that the distortions change linearly from element to element in a 64×64 matrix where each element represents approximately 6 mm and the tube-to-tube spacing is ~76 mm. Within each 6-mm element, the distortion corrections are bilinearly interpolated. The normal bilinear interpolation equations can be rearranged and expressed in the following form

$$\Delta X = C_1 + C_2 \cdot R_x + C_3 \cdot R_y + C_4 \cdot R_x \cdot R_y$$

$$\Delta Y = C_5 + C_6 \cdot R_x + C_7 \cdot R_y + C_8 \cdot R_x \cdot R_y$$

where $\Delta X, \Delta Y$ are the correction displacements, R_x and R_y are the lower 6 bits (residuals) of the digitized signals, and $C_1, C_2, \ldots, C_8$ are the correction coefficients (see Fig. 1). The lower 6 bits of each X and Y coordinate are used for the interpolation within a 6-mm element using multiplying digital-to-analog converters (MDAC). These analog outputs are summed with the original X and Y coordinates to give the true event locations.

The interpolation must be performed with sufficient accuracy to avoid introducing artifacts. Note that this implementation not only shifts a 6-mm element to a new location, but also allows a change in size and shape of each element, as shown in Fig. 2. Thus the count density within a 6-mm element will be changed gradually. Hence

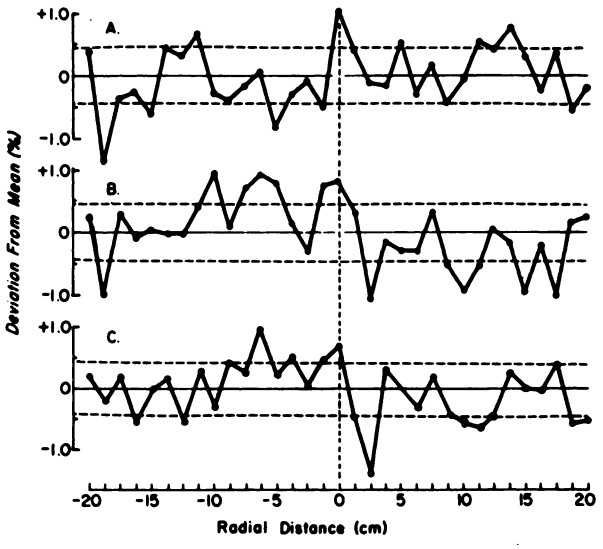

FIG. 3. Point-source sensitivity variations. Variation in count rate across face of scintillation camera measured with a point source along: (A) Y axis; (B) 45° diagonal; and (C) X axis. Percent deviation about mean is plotted as a function of position. Dashed lines (- - -) indicate one standard deviation. Nuclide was Co-57 and 20% energy window was used.

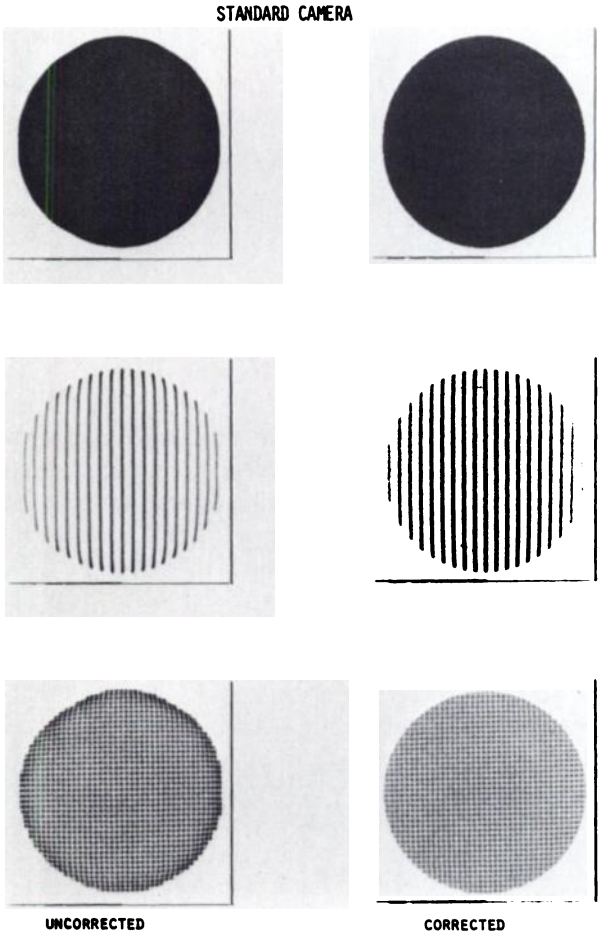

FIG. 4. Standard camera. Flood, slit-pattern, and orthogonal-hole phantom images (5, 1.5, and 2.5 million cts, respectively), with and without correction. Nuclide was Co-57, and 20% energy window was used.

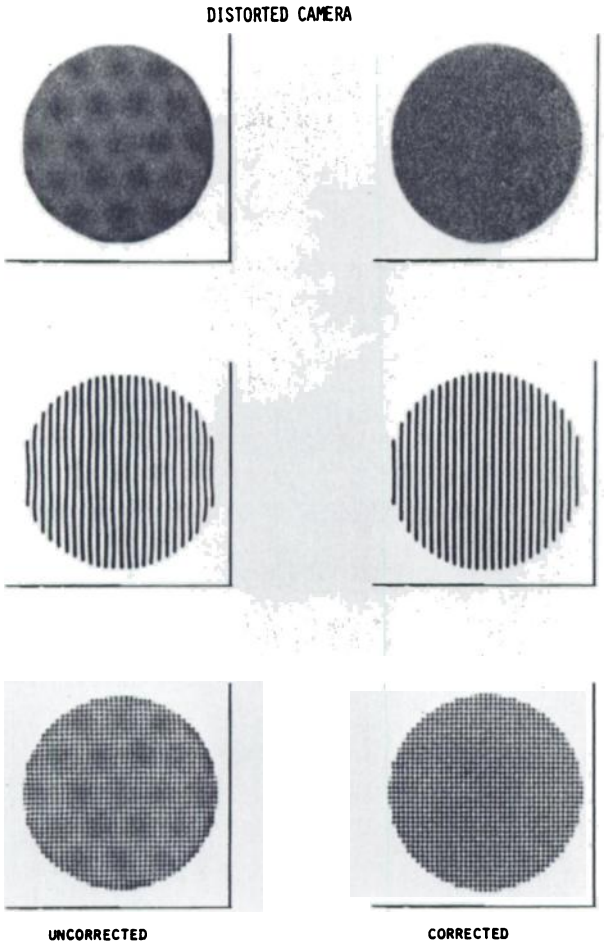

FIG. 5. Highly distorted camera. Flood, slit-pattern, and orthogonal-hole pattern images (5, 1.5, and 2.5 million cts, respectively), with and without correction. Nuclide was Tc-99m, and 15% energy window was used.

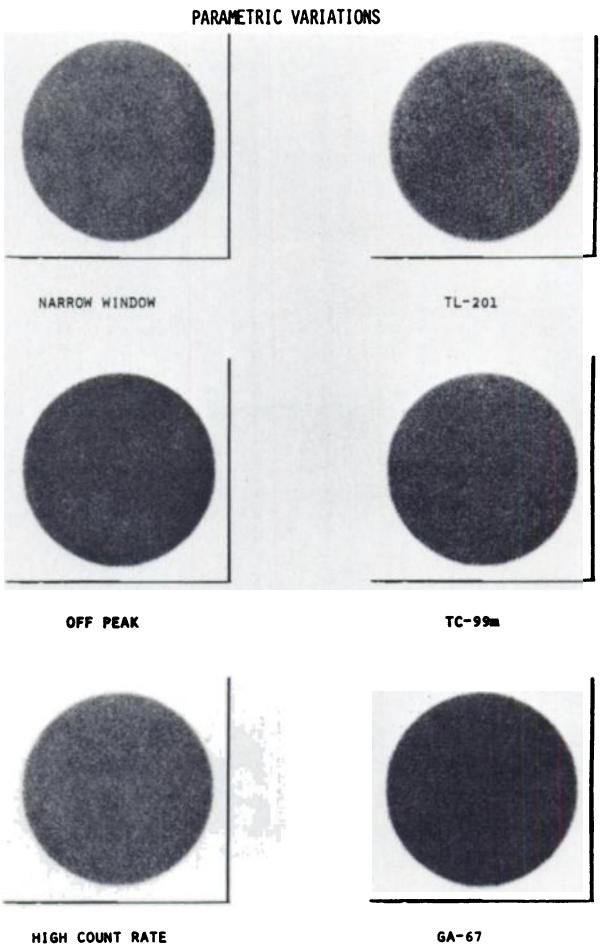

FIG. 6. Parametric variations using highly distorted camera. Flood images with Tc-99m and (A) window width at 10%; (B) window shifted off peak, 5% above correct energy; (C) count rate of 75 Kcps (low-count-rate mode); Flood images of (D) Tl-201, (E) Tc-99m, and (F) Ga-67. Five million counts were accumulated for each image.

the system avoids sudden changes in density between elements, which would otherwise be perceived easily in the final image.

Coefficient calculation. To obtain the distortion coefficients, a method consisting of two parts is used. First, the distortions are measured using a lead mask, 3 mm in thickness, with 1-mm parallel slits cut every 15 mm over the useful diameter of the camera. This pattern is placed on the crystal and can be accurately rotated 90° to obtain distortion measurements in both X and Y directions. Image data are digitized and stored in a 256 × 256 matrix; sufficient counts are accumulated to achieve a peak count of approximately 2,000 cts for each peak. The location of the peak is determined by linear interpolation between the points surrounding the half-height value. While it would be more accurate to fit a curve to all the data points, we have found that using only data points near the half-height value does not introduce significant errors given adequate counts. From the measured peak locations, an average slit spacing is calculated. The differences between the true locations obtained from the average slit spacing and the measured locations give the displacement values in both X and Y directions in an array of two 27 × 64 matrices—i.e., a measured value every 15 mm across a camera diameter of 400 mm. These matrices of displacement values are expanded to 64 × 64 matrices using a cubic spline curve fitting routine. This interpolation is justified as long as the spatial distortions change gradually from one photomultiplier center to the next, or gradually over the face of the camera (edge packing and barrel distortion).

Second, the displacement values are refined through the use of field-flood images in which distortions appear as elevated or reduced count densities. The values are iteratively modified by using the gradient of the corrected flood-field intensity as an indicator of the direction and strength of the residual distortion at each point (*14*). This second step is necessary for two reasons: (a) the X and Y distortions are coupled and cannot truly be measured independently by the line pattern; and (b) the 15-mm sampling distance (slit spacings) may not be

adequate to measure localized distortions.

The correction coefficients $C_1, C_2, \ldots, C_8$ are then calculated from the displacement values. This last step is equivalent to rearranging the bilinear interpolation formula.

PERFORMANCE

Applying distortion removal as a form of uniformity correction assumes that sensitivity variations are small and that distortions are the major cause of nonuniformities. Figure 3 shows typical count-rate profiles across the face of a well-tuned scintillation camera at various angles, as measured with a point source. At each point the data were accumulated for 10 sec at a count rate of ~6300 cps. The values are expressed as percent deviation from the mean. As can be seen, the variations are well below ±2%. It must be realized, however, that this response is a function of the camera design and will vary among cameras from different manufacturers.

To test the method, images were obtained from two cameras. One camera was an unmodified large-field camera‖ and the second was a highly distorted, "worst-case" camera obtained by modifying the light pipe. Care was taken to ensure that energy and sensitivity variations were minimized by properly tuning the cameras and by accumulating data with a symmetrical window. Images of flood, slit pattern, and orthogonal test pattern are shown for each camera with and without correction (Figs. 4 and 5). The flood images contain 5 million counts to ensure demonstration of even minor variations in uniformity. Tube-centered areas of increased activity, visible in the uncorrected images from the highly distorted camera, are not present in the corrected images. This indicates that these areas result from spatial distortions rather than sensitivity variations. Improvements with the standard camera, although not as dramatic, are visible, indicating that distortion removal can be valuable when used with present cameras as well. For each flood, integral and differential uniformity parameters were also calculated according to NEMA specifications (*15*), and are tabulated in Table 1.

TABLE 1. NEMA UNIFORMITY MEASURES FOR UNCORRECTED AND CORRECTED FLOODS

	Integral uniformity		Differential uniformity	
	UFOV*	CFOV†	UFOV*	CFOV†
Standard camera				
Uncorrected	16.0	6.8	9.3	3.9
Corrected	4.0	3.6	4.1	2.9
Highly distorted camera				
Uncorrected	13.7	13.5	12.1	12.1
Corrected	6.7	5.5	4.0	4.0

* UFOV = useful field of view.
† CFOV = central field of view.

TABLE 2. NEMA UNIFORMITY MEASURES VS. PARAMETRIC VARIATIONS

Parameter	Integral uniformity		Differential uniformity	
	UFOV*	CFOV†	UFOV*	CFOV†
Window width				
10%	6.9	6.2	3.9	3.9
15%	6.7	5.5	4.0	4.0
20%	6.4	5.9	4.3	3.6
Window shift				
−5%	9.3	6.9	6.6	4.8
0%	6.7	5.5	4.0	4.0
+5%	9.0	7.7	5.2	5.2
Count rate				
25 K cps	6.3	6.0	4.1	4.1
50 K cps	6.4	6.0	4.7	3.9
75 K cps	8.0	6.8	4.9	4.8
Nuclide				
Tl-201	9.1	8.1	4.9	4.9
Tc-99m	6.7	5.5	4.0	4.0
Ga-67	6.4	5.6	3.9	3.9

* UFOV = useful field of view.
† CFOV = central field of view.

A number of parameters can influence the distortions in the camera and therefore the accuracy of the correction. While it is possible, of course, to obtain sets of correction coefficients that match clinical conditions, it is highly desirable to choose a camera design such that a single set of coefficients is suitable over a wide range of conditions. The following parameters were investigated in detail:

1. Variations as a function of energy window width.
2. Variations as a function of window position (i.e., offset windows).
3. Variations as a function of count rate.
4. Variations as a function of photon energy (nuclide).

Figure 6, which shows examples of field floods from the "worst-case" camera, demonstrates that flood uniformity is largely impervious to parametric variations. Note that all floods were obtained without changing the set of distortion coefficients. Integral and differential uniformity parameters were also calculated and are tabulated in Table 2.

Studies are currently under way to determine the frequency with which a new coefficient set would have to be calculated. We have not found any deterioration of a camera flood after 6 mo of continuous operation. We have also dismantled a camera, moved it, and set it up again in a new location, and found that the coefficient set did not need to be updated. These preliminary studies

indicate that recalculation of the coefficient set needs to be done very infrequently if at all.

SUMMARY

The flood uniformity of scintillation cameras has been improved significantly through on-line distortion removal. This approach repositions each event to its true location and thus corrects for systematic errors, rather than compensating for such errors by adding or subtracting counts, as is done in other techniques. The method has been found to be stable with respect to parametric variations, such as energy-window width, energy-window position, count rate, and photon energy. While it is possible to update the distortion coefficients, this has not been necessary in our experience.

FOOTNOTES

† Muehllehner G: Radiation imaging device. US Patent No. 3745345, July 1973.

‡ Incorporated in the Searle Radiographics ZLC camera.

‖ Searle Radiographics, LFOV 1979.

ACKNOWLEDGMENTS

The help of P. C. Lee, A. Del Medico, and W. Luthardt was essential in reducing these concepts to practice, and their contribution is gratefully acknowledged.

REFERENCES

1. TODD-POKROPEK AE, ERBSMAN F, SOUSSALINE F: The non-uniformity of imaging devices and its impact in quantitative studies. In *Medical Radionuclide Imaging,* vol 1, Vienna, IAEA, 1977, pp 67-84
2. WICKS R, BLAU M: Effect of spatial distortion on Anger camera field-uniformity corrections: concise communication. *J Nucl Med* 20: 252-254, 1979
3. WOLFF JR: Calibration methods for scintillation camera systems. In *Quantitative Organ Visualization in Nuclear Medicine.* Coral Gables, University of Miami Press, 1971, pp 229-259
4. GRAHAM LS, OLCH A, USLER JM, et al: Automatic field uniformity corrections in scintillation cameras. *SPIE* 152: 127-131, 1978
5. MORRISON LM, BRUNO FP, MAUDERLI W: Sources of gamma camera image inequalities. *J Nucl Med* 12: 785-791, 1971
6. PADIKAL TN, ASHARE AB, KEREIAKES JG: Field flood uniformity correction: benefits or pitfalls? *J Nucl Med* 17: 653-656, 1976
7. JANSSON LG, PARKER RP: Pitfalls in gamma camera field uniformity correction. *Br J Radiol* 48: 408-409, 1975 (Letter to the Editor)
8. STEIDLEY JW, KEARNS DS, HOFFER PB: Uniformity correction with the Micro Z processor. *J Nucl Med* 19: 712, 1978 (abst)
9. SPECTOR SS, BROOKEMAN VA, KYLSTRA CD, et al: Analysis and correction of spatial distortions produced by the gamma camera. *J Nucl Med* 13: 307-312, 1972
10. KNOLL GF, BENNETT MC, STRANGE DR: Real-time correction of radioisotope camera signals for nonuniformity and nonlinearity. *J Nucl Med* 19: 746, 1978 (abst)
11. KNOLL GF, BENNETT MC, KORAL KF, et al: Removal of gamma camera nonlinearity and nonuniformities through real-time signal processing. In *VI International Conference on Information Processing in Medical Imaging,* Paris, in press
12. STOUB EW, COLSHER JG, LEE PC, et al: A spatial distortion correction method for gamma cameras. *J Nucl Med* 20: 608, 1979 (abst)
13. SOUSSALINE F, TODD-POKROPEK AE, RAYNAUD C: Quantitative studies with the gamma camera: correction for spatial and energy distortion. In *A Review of Information Processing in Medical Imaging,* Oak Ridge, Oak Ridge National Laboratory (ORNL/BCTIC-2), 1978, pp 360-375
14. SHABASON L, KIRCH D, LEFREE M, et al: Online digital methods for correction of spatial and energy dependent distortion of Anger camera images. In *A Review of Information Processing in Medical Imaging,* Oak Ridge, Oak Ridge National Laboratory (ORNL/BCTIC-2), 1978, pp 376-388
15. NEMA Standards publication for performance measurements of scintillation cameras. National Electrical Manufacturers Association, Washington DC, 1979